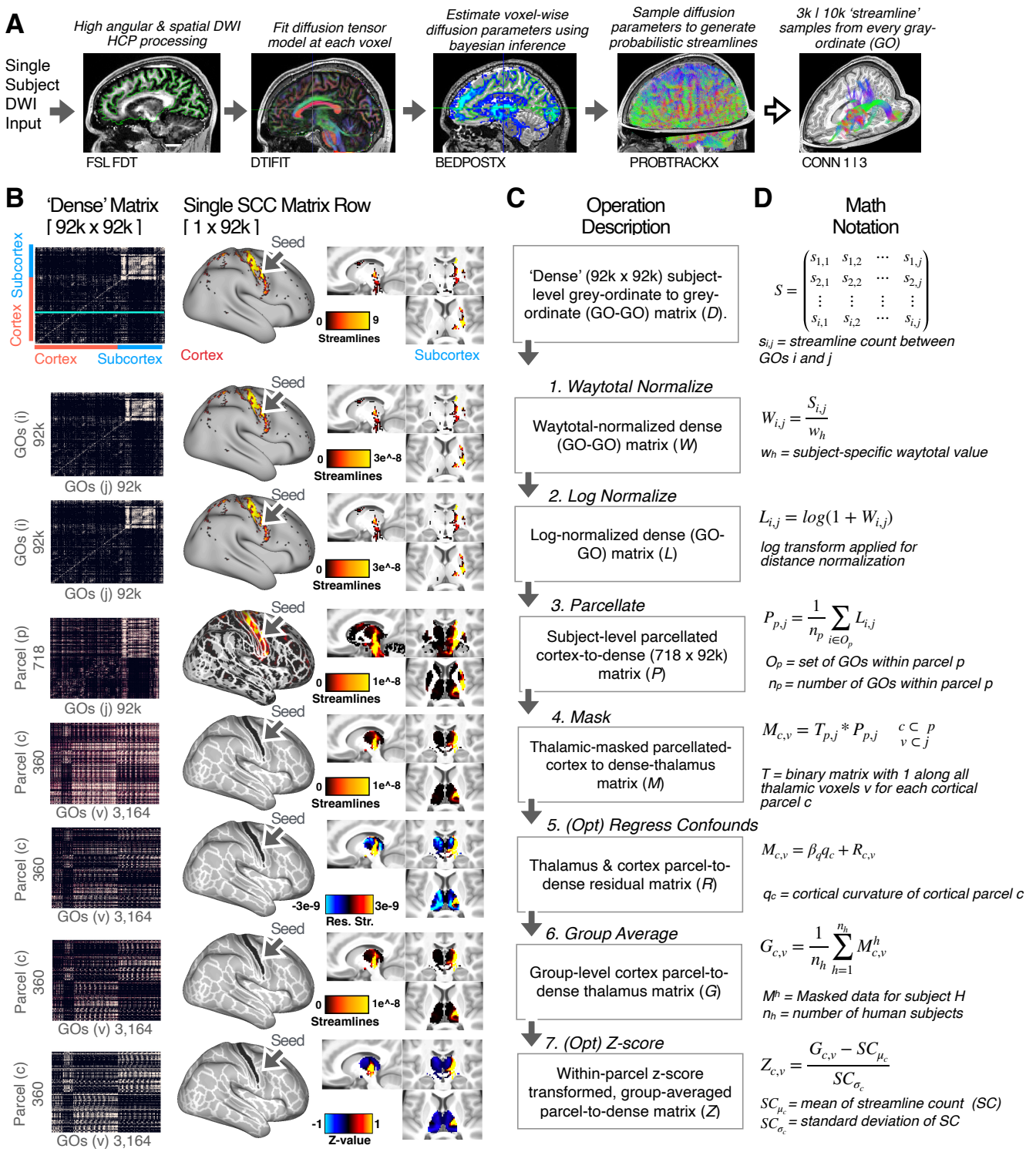

Fig. S1. Whole-brain dMRI-derived Single Subject Tractography Cortex-to-Thalamus Pipeline. Transformation of connectivity data from raw diffusion data to a normalized, whole-brain cortical-parcel to dense-thalamic connectivity matrix. These steps include (1) waytotal normalization to account for inter-subject differences in number of streamline generated (2) log normalization to account for distance effects (3) parcellation to reduce the dimensionality of the data and extract parcel by grey-ordinate streamline counts (4) masking to extract only streamline counts in the target brain area (i.e. the thalamus) (5) optional (opt) processing step to regress out cortical curvature from streamline counts (6) group averaging (7) optional step to standardize the data within each cortical parcel. This step is for visualization purposes.

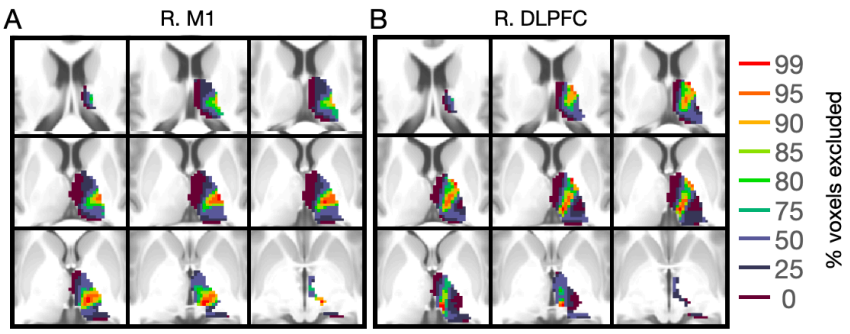

Fig. S2. Visualization of surviving thalamic voxels for a subset of exclusion thresholds for **(A)** DLPFC and **(B)** M1.

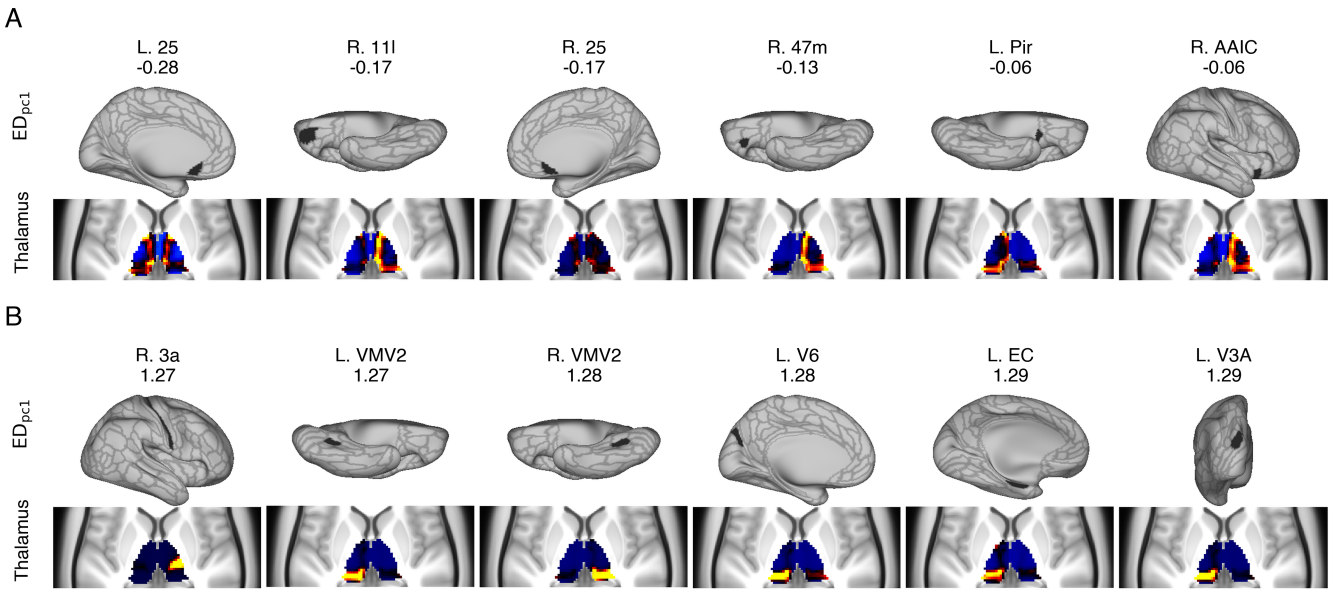

Fig. S3. Exemplar cortical parcels with some of the **(A)** lowest ipsilateral ED_{pc1} loadings and **(B)** highest ipsilateral ED_{pc1} loadings.

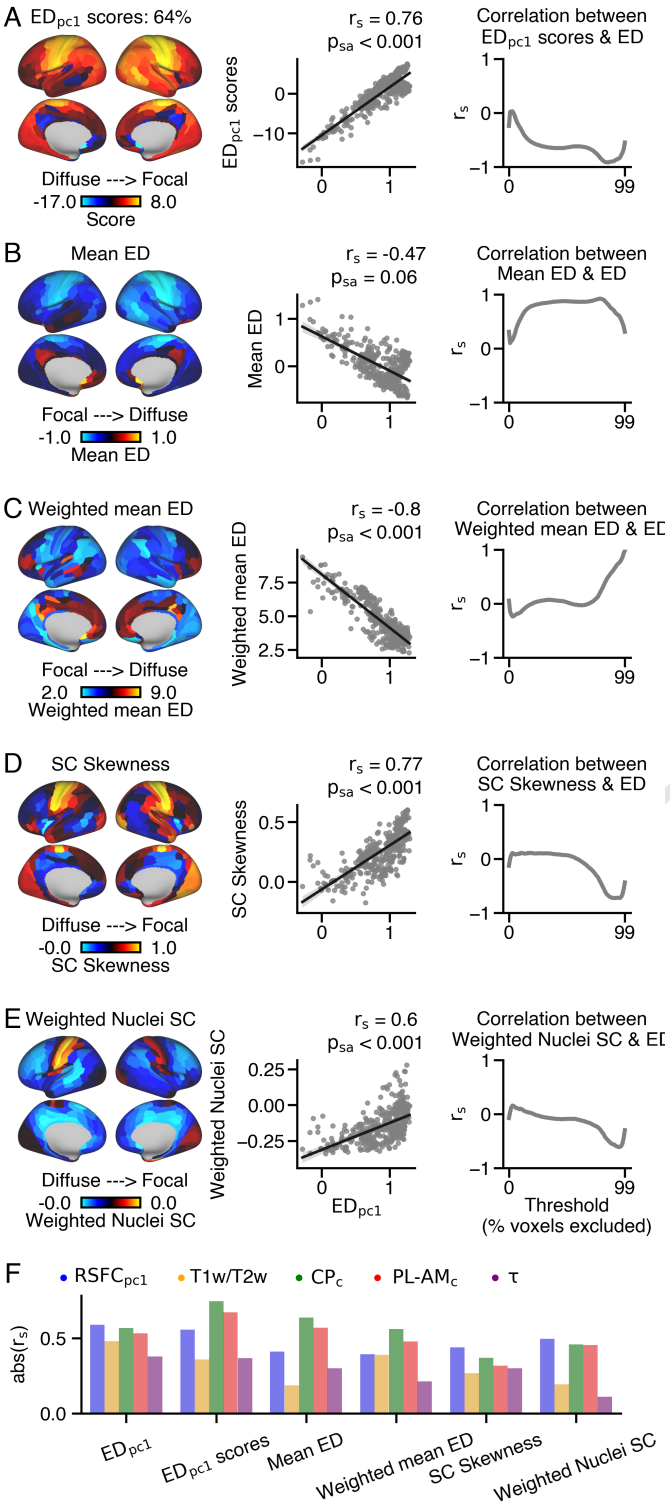

Fig. S4. Comparison of ED_{pc1} loadings with alternative measure of spatial extent. **(A)** ED_{pc1} score cortical map (left) and comparison with ED_{pc1} loadings (middle) and ED values at individual thresholds (right). PCA was applied to the transposed ED matrix (Fig. 1C) and explained 64**(B)** Mean ED value across thresholds for each cortical parcel. **(C)** Weighted Mean ED calculated by averaging thresholds with a decay function standardized between 0 and 1. **(D)** Streamline count (SC) Skewness representing the standardized difference between mean and median SC values across the thalamus. **(E)** Weighted Nuclei SC obtained by multiplying Mean SC for each cortical parcel with the corresponding thalamic nuclei volume. **(F)** Correlation comparison between cortical gradients and measures of the extent of cortical connections within the thalamus. $RSFC_{pc1}$ loadings and T1w/T2w values indicate cortical hierarchy, CP_c reflects anatomical overlap across the CALB1-PVALB thalamic gradient, PL-AM_c values reflect anatomical overlap across the anteromedial-posterolateral thalamic gradient, and τ represents intrinsic functional timescale. Refer to the main text for further details on these cortical gradients.

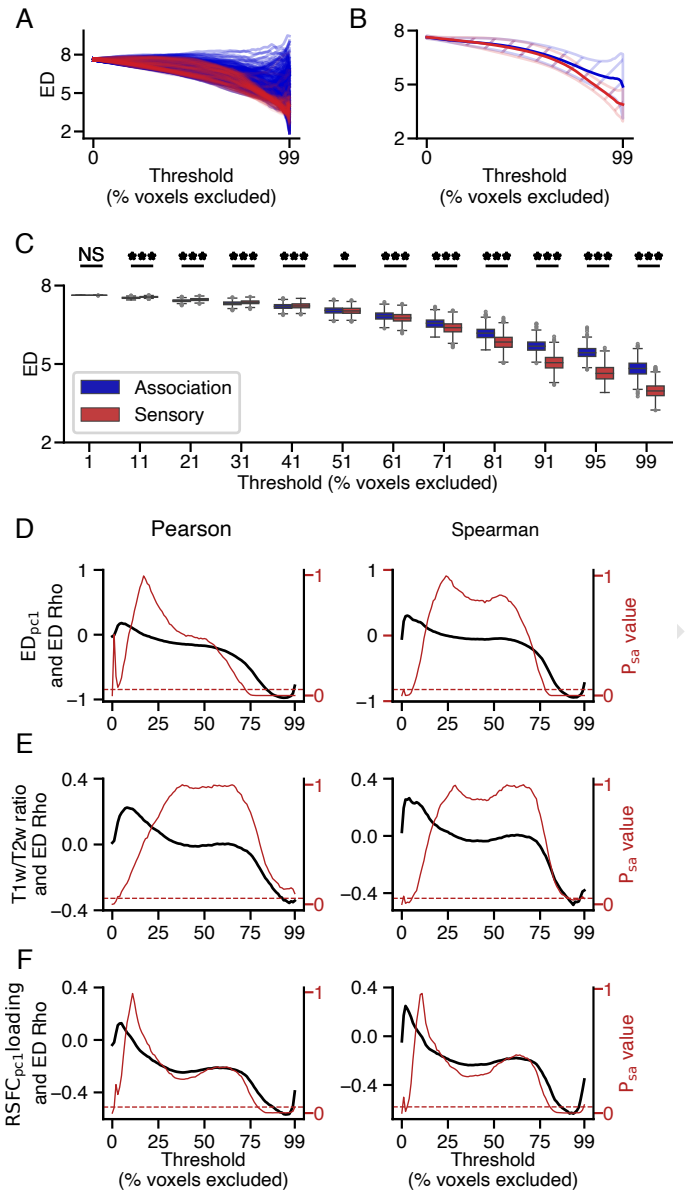

Fig. S5. Correspondence between cortical gradients and ED at different thresholds. **(A-B)** Sensory (red) and association (blue) cortical parcels exhibit distinct ED values across thresholds. (A) shows ED values across thresholds for each cortical parcel and (B) shows the average ED across thresholds for sensory and association cortical parcels, respectively. Shaded area represents the standard deviation of ED values for each threshold. **(C)** Sensory cortical parcels had significantly lower ED values for thresholds 99, 95, 91, 81, 71, 61, and 51 (Wilcoxon rank-sum test, $p < 0.001$), while association cortical parcels had significantly lower ED values for thresholds 41, 31, 21, and 11 (Wilcoxon rank-sum test, $p < 0.001$). **(D)** ED_{pc1} loadings demonstrated significant correlation with ED at more conservative thresholds (e.g., 73-99% (Pearson's rho) and 78-99% (Spearman's rank correlation)). The red dashed line indicates statistical significance at $p_{sa} < 0.05$. **(E)** T1w/T2w values exhibited significant correlation with ED at more conservative thresholds (e.g., 91-99% (Spearman's rank correlation)). **(F)** $RSFC_{pc1}$ loadings showed significant correlation with ED at more conservative thresholds (e.g., 79-99% (Pearson's correlation) and 81-98

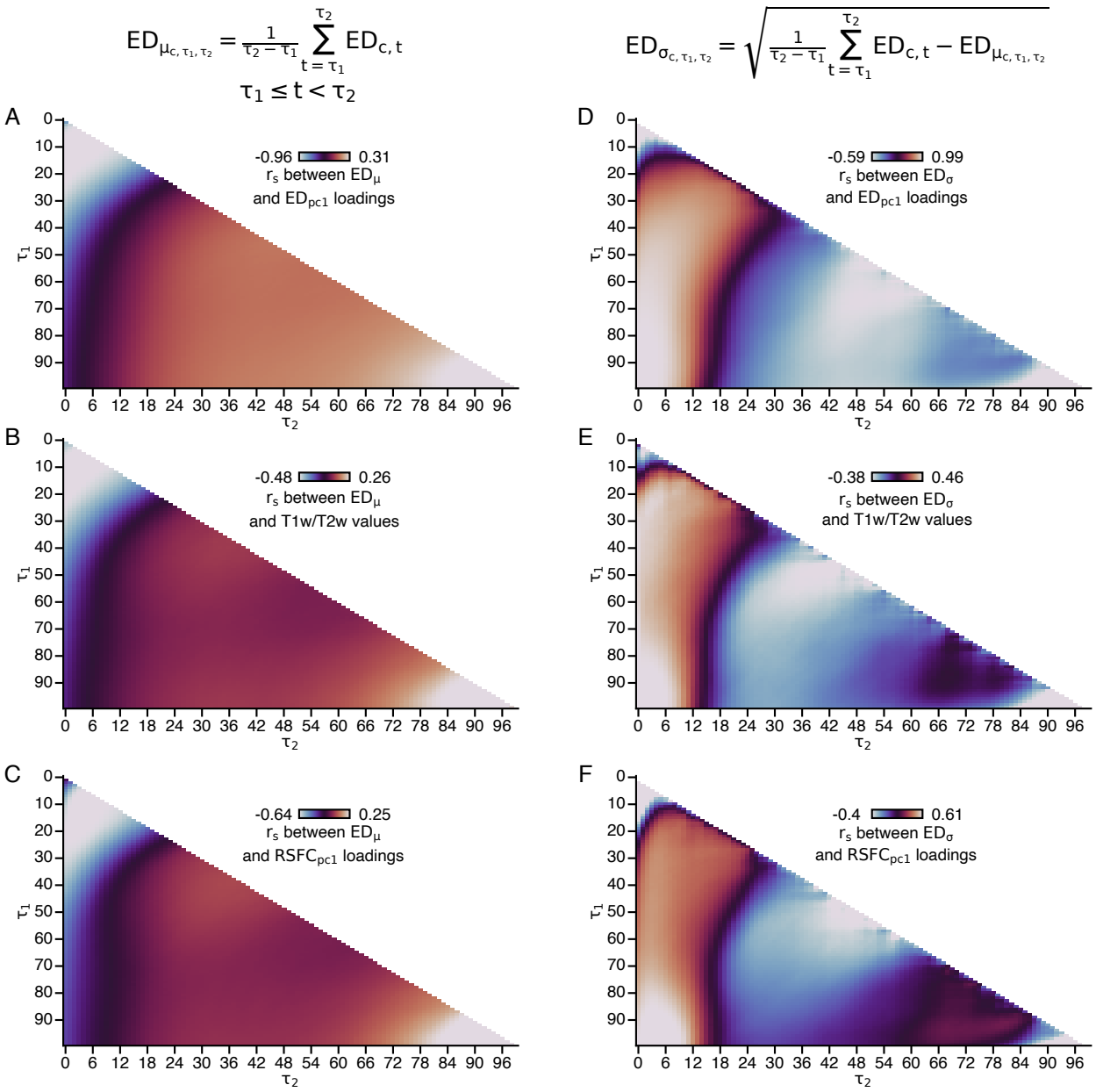

Fig. S6. Alternative threshold selection using range-based approaches to compute the mean (left panels) or standard deviation (right panels) across thresholds. **(A-C)** Mean ED values were calculated for each cortical parcel between thresholds τ_1 and τ_t, and subsequently correlated with **(A)** ED_{pc1} loadings, **(B)** T1w/T2w values, and **(C)** $RSFC_{pc1}$ loadings. **(D-E)** Standard deviation of ED values between thresholds τ_1 and τ_t was computed for each cortical parcel, and subsequently correlated with **(D)** ED_{pc1} loadings, **(E)** T1w/T2w values, and **(F)** $RSFC_{pc1}$ loadings.

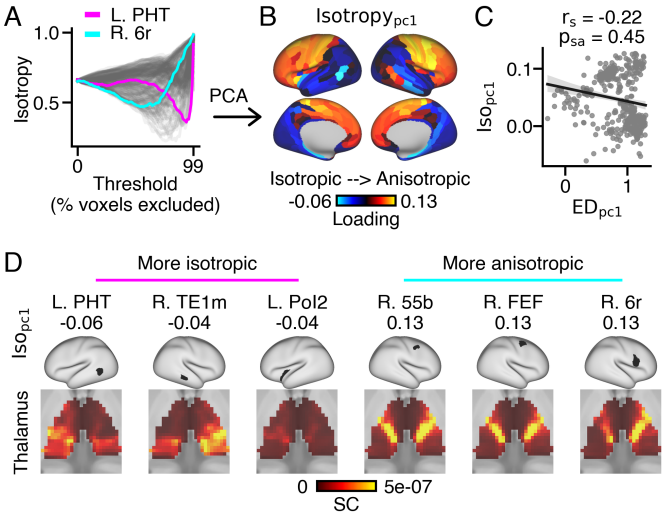

Fig. S7. Variability in the shape of thalamic connectivity patterns across cortical parcels. **(A)** Isotropy of ipsilateral thalamic connectivity patterns was calculated for each cortical parcel at 100 thresholds. Two example parcels (PHT, magenta; 6r, cyan) are shown. Lower values indicate more isotropic connectivity patterns (spread evenly in x, y, and z directions), while higher values indicate more anisotropic connectivity patterns (uneven spread in x, y, and z directions). **(B)** PCA was performed using the matrix in panel A, resulting in a single value ($Isotropy_{pc1}$ loadings) for each cortical parcel. Lower values indicate cortical parcels with more isotropic thalamic connectivity patterns, while higher values indicate cortical parcels with more anisotropic thalamic connectivity patterns. **(C)** There was no strong correlation between ipsilateral ED_{pc1} and $Isotropy_{pc1}$ loadings, indicating that the overall extent of connections is not associated with how evenly these connections spread out in x, y, and z directions. **(D)** Exemplar thalamic connectivity patterns for six cortical parcels with highly isotropic or highly anisotropic thalamic connectivity patterns.

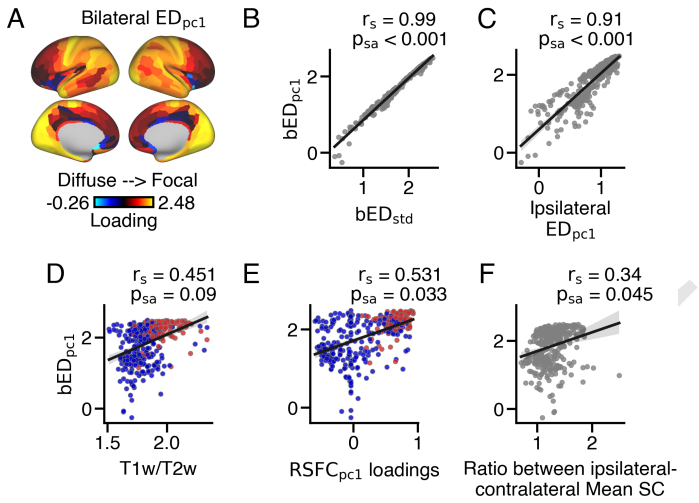

Fig. S8. Cortical variation in ipsilateral and bilateral thalamic connectivity patterns are highly conserved. **(A)** ED was calculated for right and left thalamus for each cortical parcel. The summed bilateral ED values for each parcel were subjected to PCA, yielding the first principal component (Bilateral ED_{pc1}), representing the extent of anatomical connectivity across bilateral thalamus. **(B)** Bilateral ED_{pc1} loadings exhibited a strong correlation with Bilateral ED_{σ} values. **(C)** Bilateral ED_{pc1} loadings exhibited a strong correlation with ipsilateral ED_{pc1} loadings. **(D)** Bilateral ED_{pc1} loadings exhibited a trending correlation with T1w/T2w values. **(E)** Bilateral ED_{pc1} loadings exhibited a significant correlation with $RSFC_{pc1}$ loadings. **(F)** Bilateral ED_{pc1} loadings exhibited a significant correlation with the ratio of Mean SC between ipsilateral and contralateral thalamus, reflecting the laterality of thalamic terminations. A ratio of one indicates cortical parcels with bilateral terminations, while a higher positive ratio indicates cortical parcels with predominantly ipsilateral thalamic terminations.

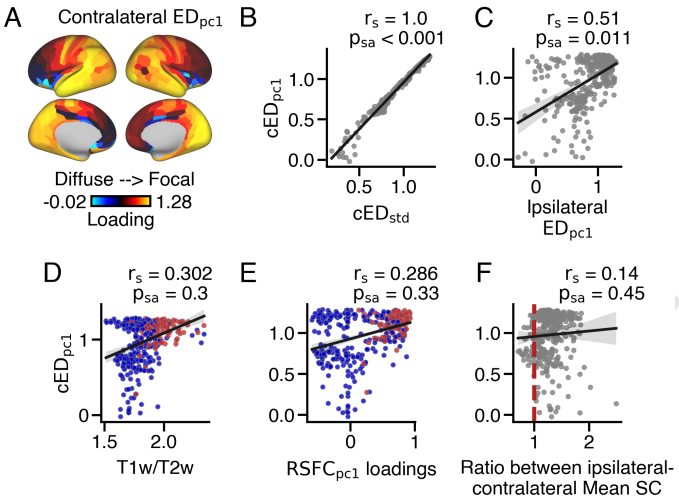

Fig. S9. Cortical variation in ipsilateral and contralateral thalamic connectivity patterns are moderately conserved. **(A)** ED was calculated for for contralateral thalamic connectivity patterns for each cortical parcel. These values were subjected to PCA, yielding the first principal component (Contralateral ED_{pc1}), representing the extent of anatomical connectivity across contralateral thalamus. **(B)** Contralateral ED_{pc1} loadings exhibited a strong correlation with contralateral ED_{σ} values. **(C)** Contralateral ED_{pc1} loadings exhibited a significant correlation with ipsilateral ED_{pc1} loadings. **(D)** Contralateral ED_{pc1} loadings did not significantly correspond with T1w/T2w values. **(E)** Contralateral ED_{pc1} loadings did not significantly correspond with $RSFC_{pc1}$ loadings. **(F)** Contralateral ED_{pc1} loadings did not have a significant correlation with the ratio of Mean SC between ipsilateral and contralateral thalamus, which indexes the laterality of thalamic terminations (i.e., a ratio less than one (red dashed lined) indexes cortical parcels with stronger contralateral thalamic connectivity). Some cortical parcels have stronger anatomical connections to contralateral thalamus relative to ipsilateral thalamus, and those cortical parcels had higher contralateral ED_{pc1} loadings.

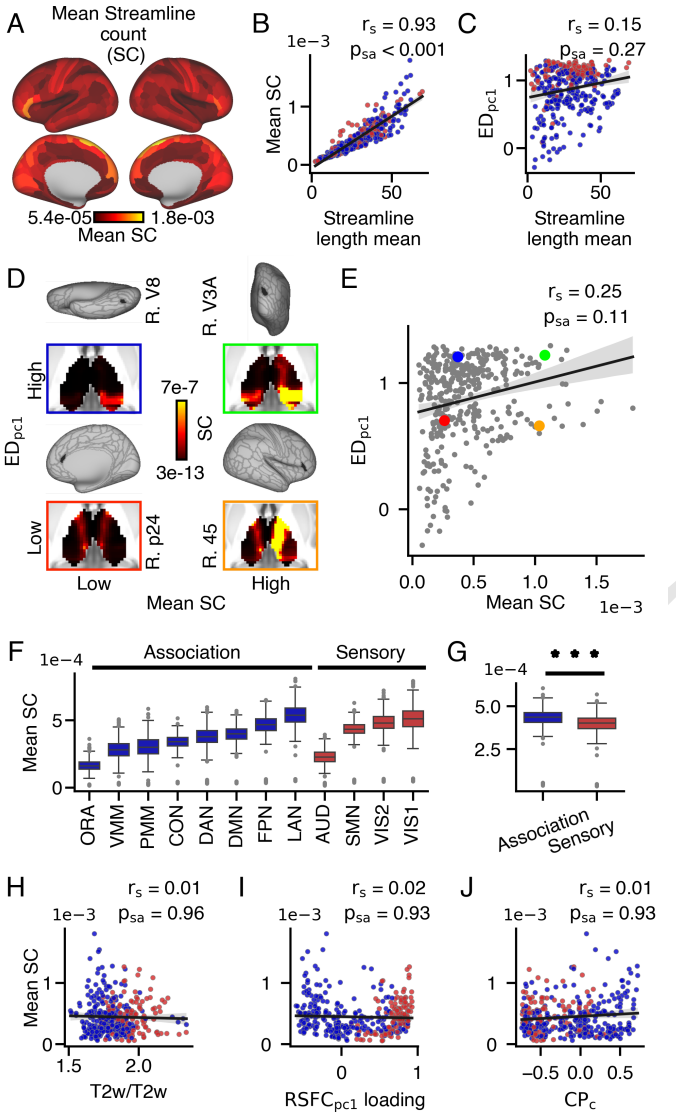

Fig. S10. Dissociation between extent and strength in thalamic connectivity patterns. **(A)** Mean streamline count (Mean SC) was computed for each cortical parcel, representing the relative strength of connectivity. Parcels with higher Mean SC values have more streamline terminations within the thalamus. **(B)** Mean SC strongly correlated with mean streamline length. **(C)** Mean streamline length weakly correlated with ED_{pc1}. **(D-E)** Exemplar cortical parcels were selected based on their low/high (R. 45; orange), high/high (R. V3A; green), low/low (R. p24; red), and high/low (R. V8; blue) ED_{pc1}/Mean SC values. **(F-G)** Mean SC varied within and between cortical networks, with slightly lower values in sensory (median = 4.0e-04) compared to association (median = 4.4e04) networks (Wilcoxon signed-rank test, p = 3.9e-94). There was no correlation between Mean SC and **(H)** T1w/T2w values, **(I)** $RSFC_{pc1}$ loadings, or **(J)** CP_c values.

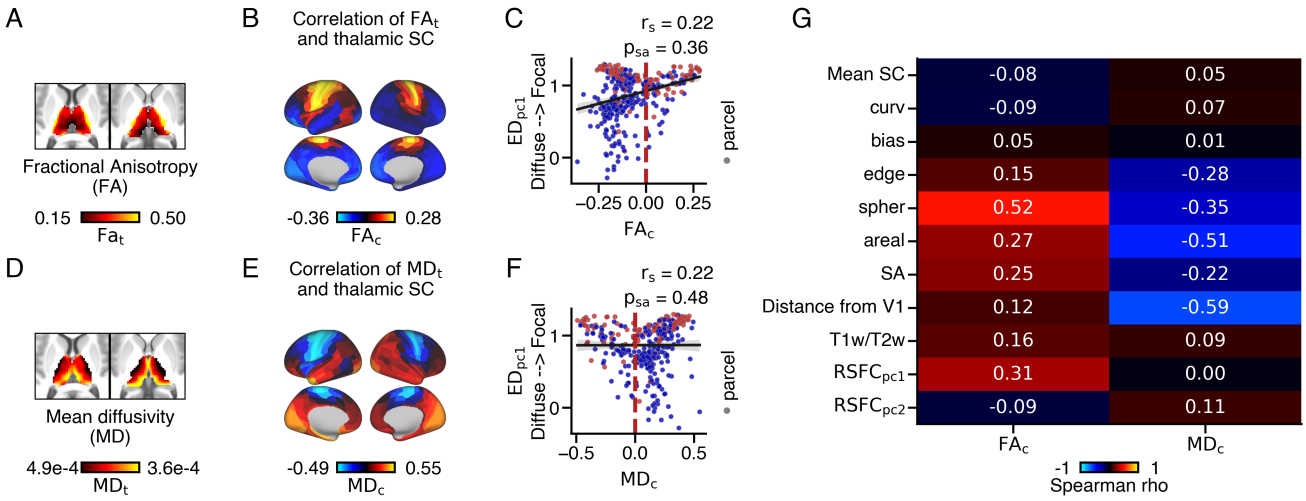

Fig. S11. Fractional anisotropy (FA_t) and mean diffusivity (MD_t) were obtained from FSL's DTIFIT and group-averaged across 828 HCP subjects. **(A)** Thalamic gradient of fractional anisotropy (FA_t). **(B)** The overlap between each cortical parcel's anatomical connectivity along the FA_t gradient was calculated for each cortical parcel. Across cortex, higher values denote cortical parcels that preferentially couple with thalamic areas with higher Fa values (Fa_c). **(C)** FA_c did not demonstrate a significant correlation with ED_{pc1} loadings (p_{sa} = 0.36). **(D)** Thalamic gradient of mean diffusivity (MD_t). **(E)** The overlap between each cortical parcel's anatomical connectivity along the Md_t gradient was calculated for each cortical parcel. Across cortex, higher values denote cortical parcels that preferentially couple with thalamic areas with higher Md values (MD_c). **(F)** MD_c did not exhibit a significant correlation with ED_{pc1} loadings (p_{sa} = 0.48). **(G)** correlation between FA_t and MD_t with cortical gradients. Fractional anisotropy overlap values showed the highest correlation with spherical distortion, while mean diffusivity exhibited the highest correlation with distance from V1 and areal distortion.

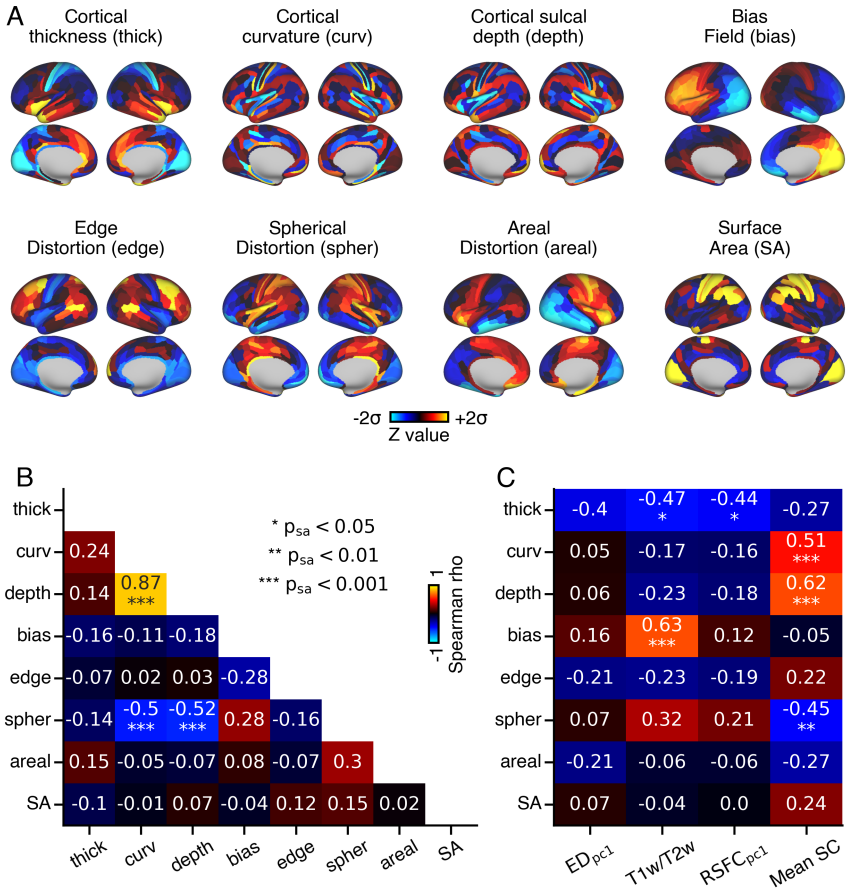

Fig. S12. ED_{pc1} loadings show no correlation with measures of cortical geometry, bias, and distortion. **(A)** Cortical maps illustrating cortical thickness, cortical curvature, sulcal depth, bias field, edge distortion, spherical distortion, and areal distortion. **(B)** Correlation matrix showing relationships among cortical geometry, bias, and distortion maps. **(C)** Correlations between cortical geometry, bias, and distortion maps, and ED_{pc1}, T1w/T2w, $RSFC_{pc1}$, and Mean SC values.

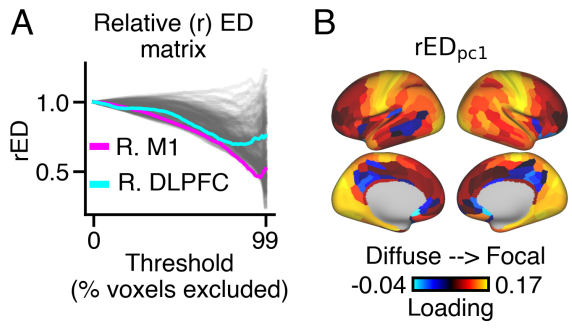

Fig. S13. Normalization of ED for shape and size differences between left and right thalamus. **(A)** To address shape differences, ED values were divided by the unthresholded ED value (when 0% of voxels were excluded) for each cortical parcel, creating a relative measure of ED. **(B)** Cortical map of relative (r) rED_{pc1}. **(C)** rED_{pc1} and ED_{pc1} exhibited a nearly perfect correlation.

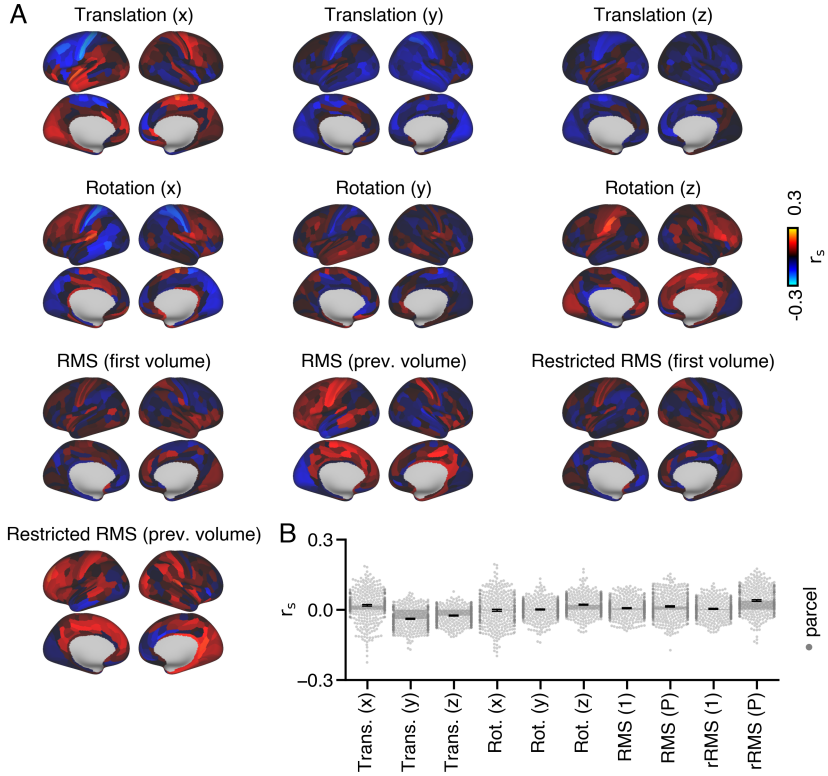

Fig. S14. Absence of systematic bias in ED_{pc1} loadings due to motion. Motion estimates, including translation and rotation in x, y, and z directions, were extracted from FSL's Eddy tool. RMS (root mean square) and restricted RMS measures were obtained for 813 subjects. These estimates were averaged across volumes, resulting in 10 motion measures per subject. Correlations were then computed between these motion measures and ipsilateral ED_{pc1} loadings for each cortical parcel separately. **(A)** This process yielded 360 Spearman's rho values for each motion parameter. **(B)** Weak correlations were observed between ED_{pc1} loadings and motion estimates across all cortical parcels. The mean correlation between ED_{pc1} loadings and all motion parameters was close to zero, indicating the absence of systematic bias due to translation or rotation in x, y, or z directions, as well as total movement.

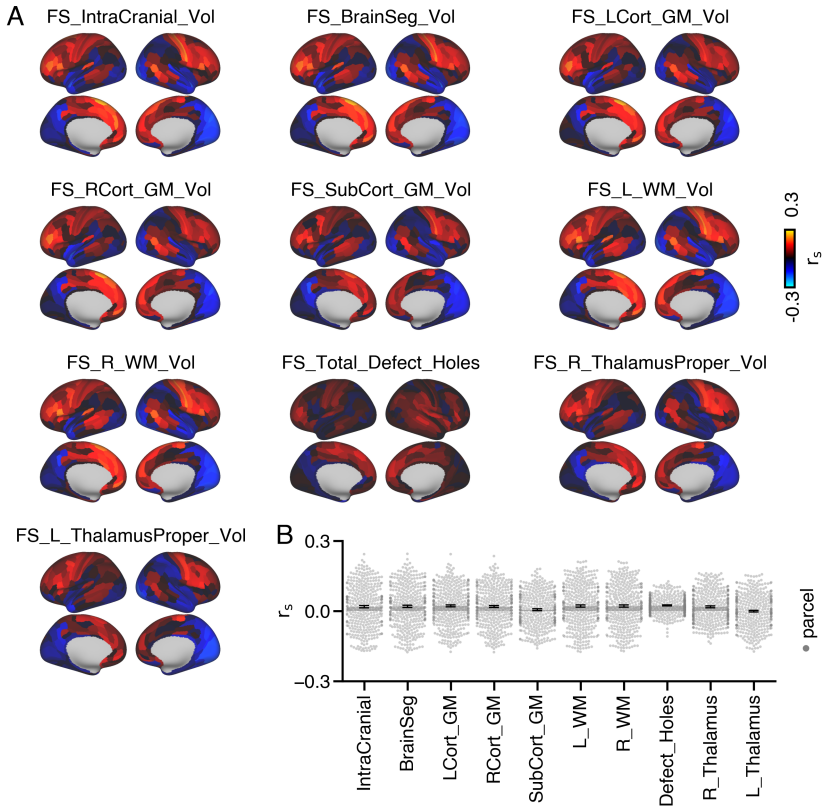

Fig. S15. Absence of correspondence between ED_{pc1} loadings and individual variation in white matter (WM), gray matter (GM), or defects. Freesurfer measures, including intracranial volume, brain segmentation volume, GM and WM volumes for left and right cortex, subcortical GM volume, total defect holes, and total volume of left and right thalamus, were obtained from the HCP's ConnectomeDB. Correlations were computed between these 10 Freesurfer measures and ipsilateral ED_{pc1} loadings for each cortical parcel, separately. **(A)** This process resulted in 360 Spearman's rho values for each Freesurfer measure. **(B)** Weak correlations were observed between ED_{pc1} loadings and Freesurfer measures across all cortical parcels. The mean correlation between ED_{pc1} loadings and all Freesurfer measures was close to zero, indicating the absence of systematic bias by individual variation in WM or GM volumes in cortex, subcortex, or thalamus.

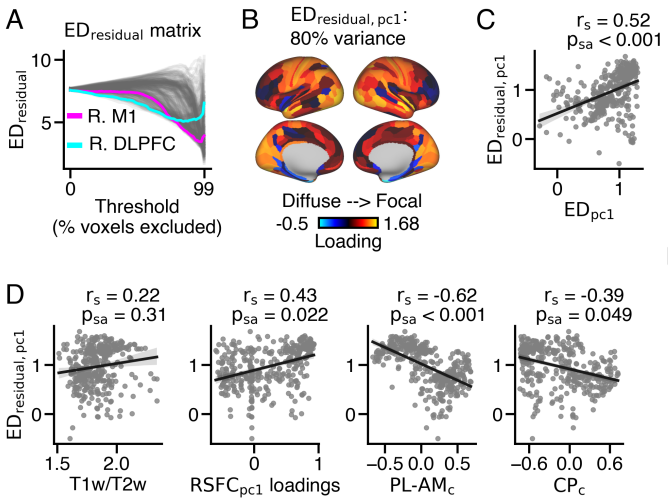

Fig. S16. Correspondence between pre- and post-regression ED_{pc1} values after removing cortical curvature from streamline counts. Cortical curvature was regressed from each subject's streamline count connectivity matrix, and the residuals were group-averaged for further analysis using the multithresholding framework. **(A)** $ED_{residual}$ was calculated on surviving thalamic voxels with the highest residual streamline count for each threshold. **(B)** PCA was performed on the $ED_{residual}$ matrix, and the first principal component ($ED_{residual,pc1}$ loadings) accounted for 80**(C)** Significant correlation was observed between ED_{pc1} (derived from streamline counts) and $ED_{residual,pc1}$ (derived from residual streamline counts) loadings. **(D)** $ED_{residual,pc1}$ loadings did not correspond with cortical myelin, but exhibited significant correlations with $RSFC_{pc1}$ loadings, $PL\text{-}AM_c$ values, and CP_c values.

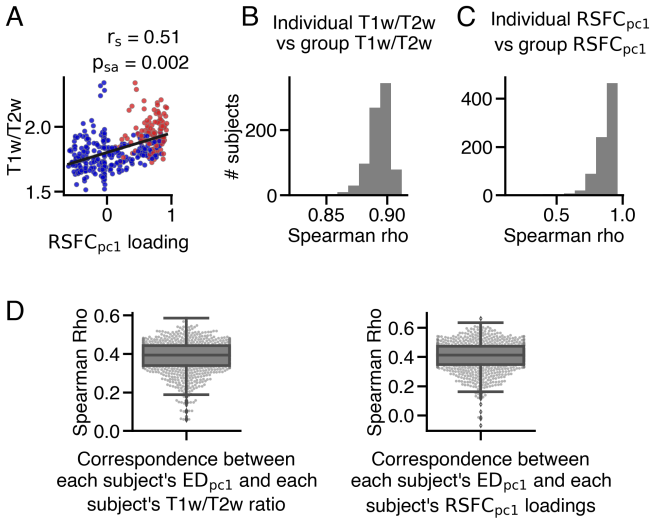

Fig. S17. **(A)** Group-averaged T1w/T2w values and $RSFC_{pc1}$ loadings exhibited a significant positive correlation across the cortex. Sensory cortical parcels are represented by red dots, while association cortical parcels are represented by blue dots. **(B)** Individual subjects' T1w/T2w values closely resembled the group-averaged values (mean: 0.89, median: 0.89, SEM = 0.0003, STD = 0.009). **(C)** Individual subjects' $RSFC_{pc1}$ loadings showed high similarity to the group-averaged loadings on average (mean: 0.87, median: 0.89, SEM = 0.0003, STD = 0.08). **(D)** Hierarchical variation in ED_{pc1} loadings remained consistent across subjects. Individual subjects' ED_{pc1} loadings exhibited correlations with their respective T1w/T2w ratio (mean: 0.38, median: 0.39, SEM = 0.003, STD = 0.08) and $RSFC_{pc1}$ loadings (mean: 0.40, median: 0.41, SEM = 0.003, STD = 0.10) using Spearman correlation.

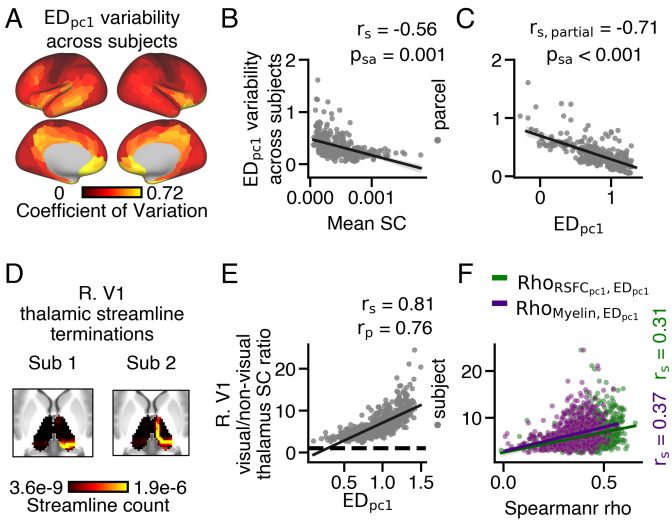

Fig. S18. Variability of the extent of cortical connections within the thalamus across individuals. **(A)** The coefficient of variation of ED_{pc1} was calculated for each cortical parcel, quantifying inter-subject variability while accounting for the overall extent of cortical connections within the thalamus. **(B)** Across the cortex, the variability of ED_{pc1} loadings exhibited a negative correlation with Mean SC, indicating that cortical parcels with higher streamline terminations had lower inter-subject variability. **(C)** The variability of ED_{pc1} loadings across subjects positively correlated with group-averaged ED_{pc1} loadings, even after accounting for Mean SC. **(D)** Exemplar thalamic connectivity patterns from right V1 for two subjects, demonstrating focal (sub 1) and diffuse (sub 2) patterns. While both subjects showed terminations in the visual thalamus (e.g., posterior thalamus; pulvinar and lateral geniculate nucleus), subject 2 displayed additional terminations extending to the anterior thalamus, potentially indicating false positives (112). **(E)** The ratio of streamline counts from right V1 to visual thalamus (pulvinar and lateral geniculate nucleus) relative to non-visual thalamus (other thalamic nuclei) highly correlated with right V1 ED_{pc1} loadings across subjects. **(F)** The ratio of right V1 streamline terminations to visual and non-visual thalamus was compared to individual Spearman correlation coefficients (ρ) between ED_{pc1} and T1w/T2w (purple) and $RSFC_{pc1}$ (green) values.

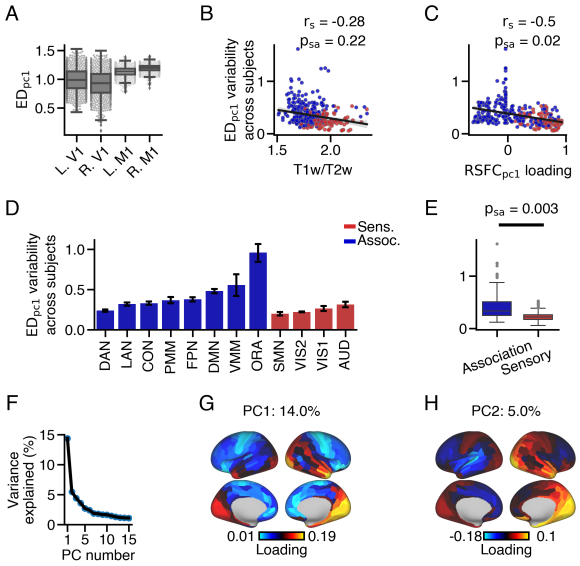

Fig. S19. **(A)** Exemplar ED_{pc1} loadings for left and right visual area 1 (V1) and M1, highlighting higher inter-subject variation in V1 compared to M1. Across the cortex, the variability of ED_{pc1} across subjects did not strongly correspond with **(B)** T1w/T2w values, but **(C)** exhibited a correlation with $RSFC_{pc1}$ loadings. **(D-E)** Furthermore, the variability of ED_{pc1} loadings across subjects differed significantly between sensory and association cortical networks. **(F-H)** Principal Component Analysis (PCA) was conducted using a subject-by-cortical parcel (828 x 360) matrix of ED_{pc1} loadings to identify major axes of inter-subject variation in the extent of cortico-thalamic anatomical patterns. **(F)** Scree plot showing the eigenvalues. **(G)** The first principal component (PC1) accounted for 14% of the variation across subjects. **(H)** The second principal component (PC2) explained 5% of the variation across subjects.

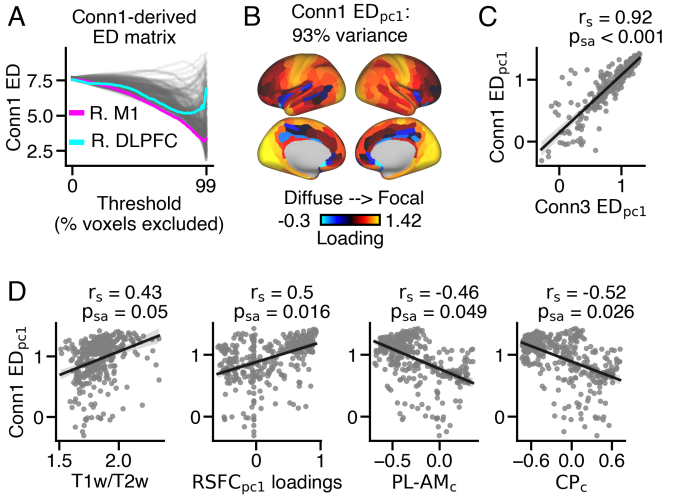

Fig. S20. Comparison of ED_{pc1} loadings derived from bidirectional white-ordinate to gray-ordinate (Conn3) and unidirectional gray-ordinate to gray-ordinate (Conn1) seeding strategies. **(A)** ED matrix derived from Conn1 seeding strategy. **(B)** ED_{pc1} loading map derived from Conn1 seeding strategy. PCA was performed on the Conn1-derived ED matrix, resulting in 360 loadings from the first principal component (PC1), which accounted for 93**(C)** Strong positive correlation observed between Conn1 and Conn3-derived ED_{pc1} loadings. **(D)** Conn1-derived ED_{pc1} loadings exhibited significant correlations with T1w/T2w, $RSFC_{pc1}$, $PL\text{-}AM_c$, and CP_c values.

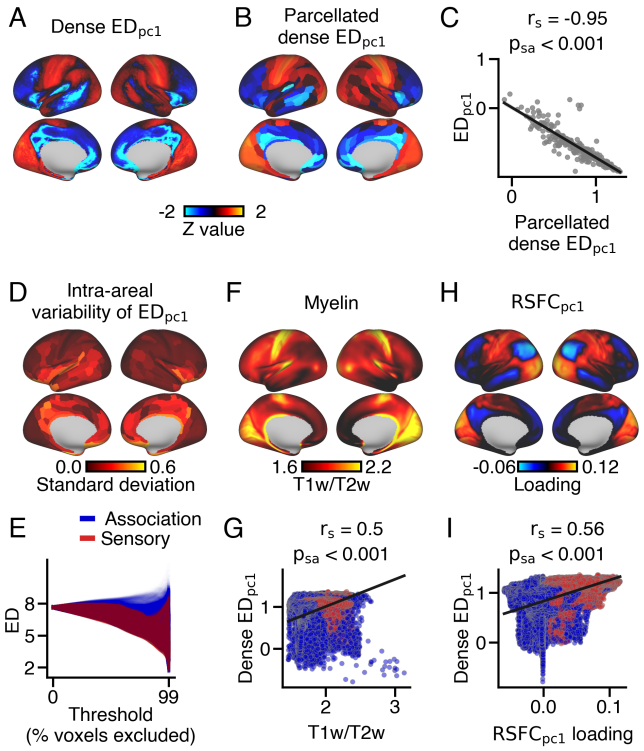

Fig. S21. ED_{pc1} loadings on dense cortical data replicate observations from parcellated cortical data. **(A)** Cortical map displaying ED_{pc1} loadings for each of the 59,412 cortical vertices (Dense ED_{pc1}). **(B)** Average of Dense ED_{pc1} loadings within 360 cortical parcels from Glasser et al. (113) (Parcellated Dense ED_{pc1}). **(C)** Parcellated Dense ED_{pc1} loadings exhibit a strong correlation with ED_{pc1} loadings calculated from parcel-level data. **(D)** Variation of Dense ED_{pc1} loadings within each cortical parcel. **(E)** ED matrix derived from group-averaged dense cortical data, displaying ED values for each cortical vertex across 100 thresholds. **(F)** Dense cortical myelin map, calculated as the average T1w/T2w value across 828 subjects. Sensory cortical vertices show higher T1w/T2w values compared to association cortical vertices. **(G)** Dense ED_{pc1} loadings exhibit a correlation with Dense T1w/T2w values across the cortex. **(H)** Loading map of the dense cortical principal functional resting-state gradient ($RSFC_{pc1}$). Sensory cortical vertices exhibit higher loadings compared to association cortical vertices. **(I)** ED_{pc1} loadings demonstrate a correlation with $RSFC_{pc1}$ loadings across the cortex.

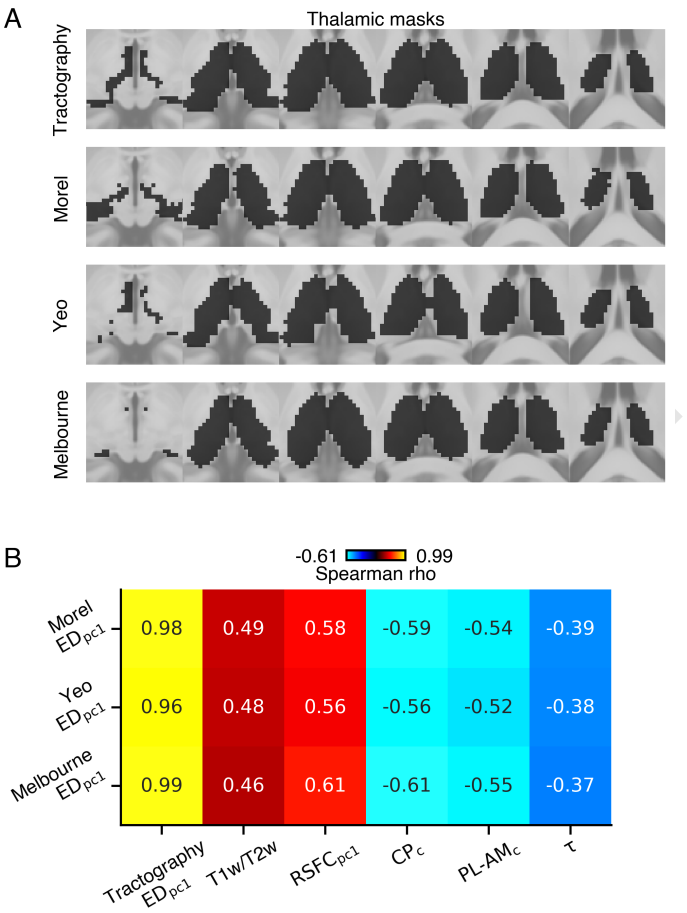

Fig. S22. Comparison of ipsilateral ED_{pc1} loadings calculated using different thalamic masks. **(A)** Binary thalamic masks: the top panel represents the mask used for tractography seeding and ED_{pc1} loadings throughout the paper, while the subsequent panels display thalamic masks derived from the Morel atlas (53), the Yeo atlas (114), and the Melbourne atlas (115). **(B)** ED_{pc1} loadings derived from each thalamic mask exhibited high similarity, as well as consistent relationships with the T1w/T2w, $RSFC_{pc1}$, CP_c, $PL\text{-}AM_t$, and τ cortical gradients.

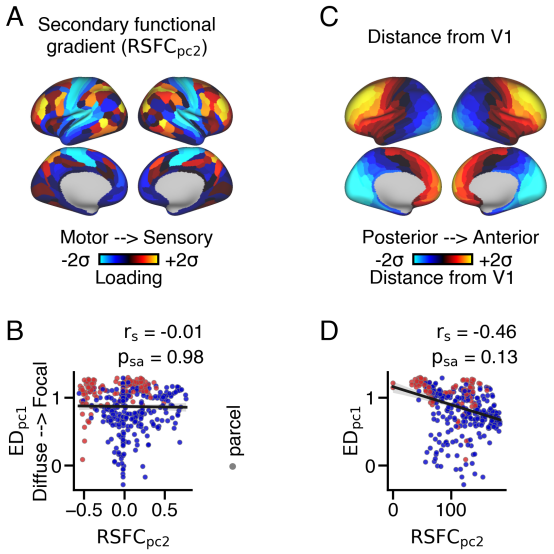

Fig. S23. **(A)** Cortical map displaying the loading values of the secondary functional resting-state gradient ($RSFC_{pc2}$), obtained through PCA analysis of group-averaged resting-state functional connectivity data. Sensory cortical parcels exhibit lower loadings compared to association and motor cortical parcels. **(B)** No significant correlation was observed across the cortex between ED_{pc1} loadings and $RSFC_{pc2}$ loadings. **(C)** Anteroposterior cortical gradient represented by the distance from visual area 1 (V1). Anterior cortical parcels demonstrate higher values compared to posterior cortical parcels. **(D)** ED_{pc1} loadings did not exhibit a significant correlation with distance from V1 values across the cortex.

Table 1. Morel thalamic nuclei names, abbreviations, classes, and volumes

Group	Name	Abbr.	Higher/First order	Phillips (56) subgroups	Volume (# 2mm voxels)
Anterior group					
	Anterior dorsal	AD	FO	AD	1
	Anterior medial	AM	HO	Secondary	15
	Anterior ventral	AV	FO	Primary	78
	Lateral dorsal	LD	FO	Primary	44
Medial group					
	Centre median	CM	HO	Tertiary	64
	Parafascicular	Pf	HO	Tertiary	73
	Central lateral	CL	HO	Tertiary	189
	Central medial	CeM	HO	Tertiary	56
	Mediodorsal	MD	HO	Secondary	310
	Paraventricular	PV	HO	Tertiary	2
	Medioventral	MV	HO	Re	9
	Habenular	Hb			22
Posterior group					
	Limitans	Li			27
	Suprageniculate	SG			18
	Lateral posterior	LP	HO	Secondary	138
	Posterior	Po	HO	Secondary	13
	Medial geniculate	MGN	FO		70
	Lateral geniculate	LGN	FO	Primary	87
	Anterior pulvinar	PuA	HO	Secondary	34
	Inferior pulvinar	PuI	HO	Secondary	18
	Lateral pulvinar	PuL	HO	Secondary	57
	Medial pulvinar	PuM	HO	Secondary	530
Lateral group					
	Ventral posterior lateral	VPL	FO	Primary	142
	Ventral posterior medial	VPM	FO	Primary	55
	Ventral posterior inferior	VPI	FO	Primary	22
	Ventral lateral	VL	FO	Primary	459
	Ventral medial	VA	HO	Secondary	192
	Ventral anterior	VM	HO	Secondary	51

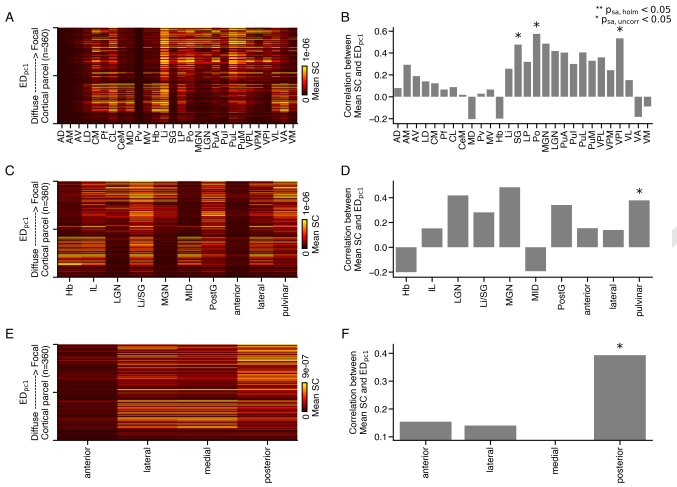

Fig. S24. (A) Streamline count (SC) connectivity matrix between each cortical parcel and thalamic nuclei (untransformed). **(B)** Correlation between ED_{pc1} loadings and mean SC within each thalamic nucleus. Cortical parcels with focal thalamic connectivity patterns exhibit preferential coupling to SG, Po, and VPl nuclei. **(C)** SC connectivity matrix between each cortical parcel and minor thalamic subdivisions. **(D)** Correlation between ED_{pc1} loadings and mean SC within each minor subdivision of the thalamus. Cortical parcels with focal thalamic connectivity patterns exhibit preferential coupling to pulvinar nuclei. **(E)** SC connectivity matrix between each cortical parcel and major thalamic subdivisions. **(F)** Correlation between ED_{pc1} loadings and mean SC within each major subdivision of the thalamus. Cortical parcels with focal thalamic connectivity patterns exhibit preferential coupling to posterior nuclei.

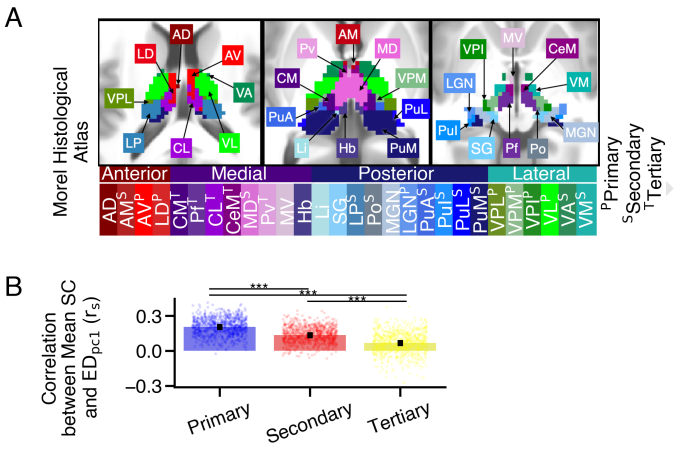

Fig. S25. Correspondence between Mean SC and ED_{pc1} for thalamic subgroups defined in Phillips et al. (2019). Thalamic nuclei were categorized into primary, secondary, tertiary, anterodorsal, and reunions subgroups based on gene expression data (56). **(A)** Morel thalamic nuclei were assigned to primary, secondary, or tertiary subgroups. **(B)** There was a significant difference in the correlation between ED_{pc1} loadings and Mean SC for primary (median: 0.21), secondary (median: 0.14), and tertiary (median: 0.07) thalamic nuclei (χ^2 (3) = 1165, p < .001). Post-hoc Nemenyi tests revealed significant differences for all group comparisons (*** p = 0.001).

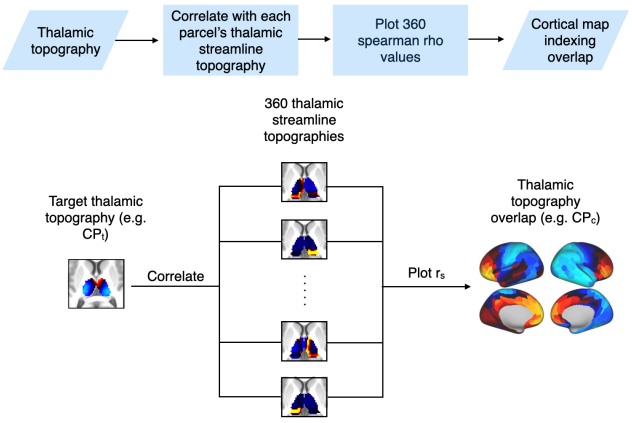

Fig. S26. Flow diagram (top panel) and workflow visualization (bottom panel) depicting the methodology used to assess the overlap between thalamic anatomical connectivity and thalamic gradients. The streamline counts of each cortical parcel within the thalamus were correlated with a target thalamic gradient, yielding a cortical map of Spearman rho values. Higher rho values indicate a stronger correspondence between a cortical parcel's thalamic anatomical connectivity patterns and positive values in the target thalamic gradient.

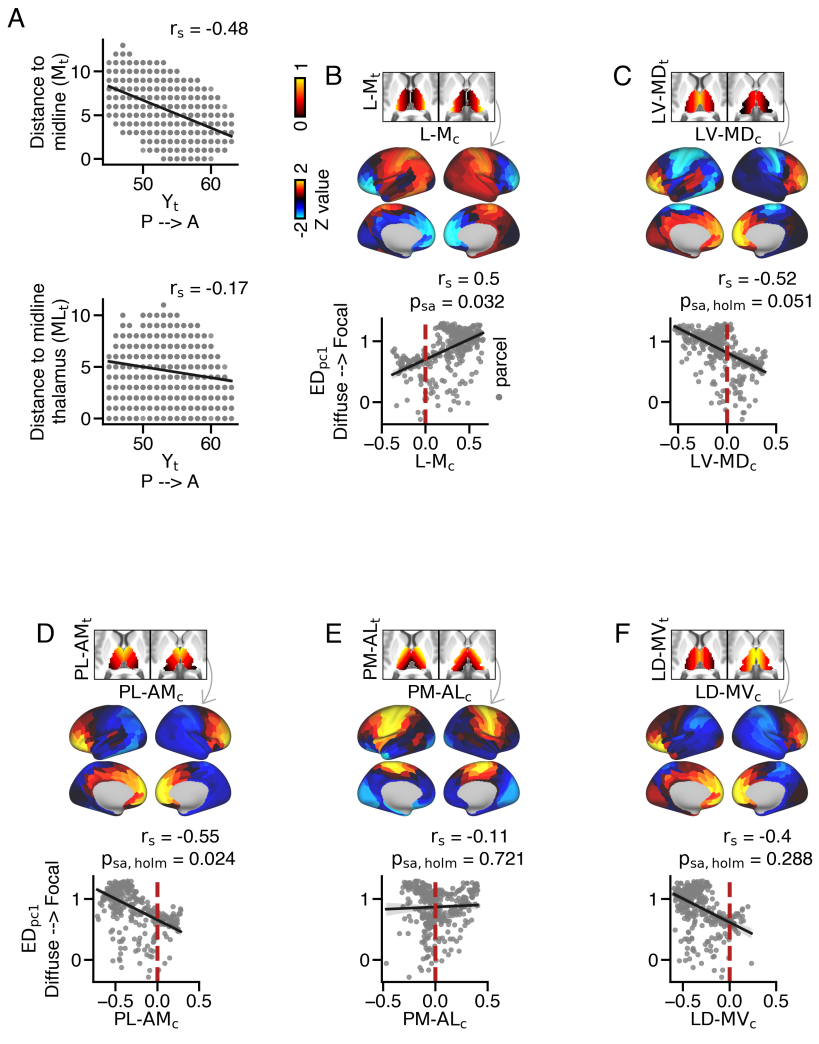

Fig. S27. Confounding effect of anteroposterior axis on distance to midline. **(A)** Position along the anteroposterior (y_t) thalamic axis showed stronger correlation with distance from midline compared to distance from thalamic midline. **(B)** There was a significant correlation between the overlap of cortical parcel's thalamic anatomical connectivity and distance to midline with ED_{pc1} loadings. **(C-F)** The overlap of cortical parcel's anatomical connectivity with thalamic spatial gradients using distance to midline as an index showed strong correspondence with **(C)** mediodorsal and **(D)** anteromedial thalamic gradients. However, **(E)** anterolateral and **(F)** medioventral thalamic gradients did not significantly correspond with ED_{pc1} loadings.

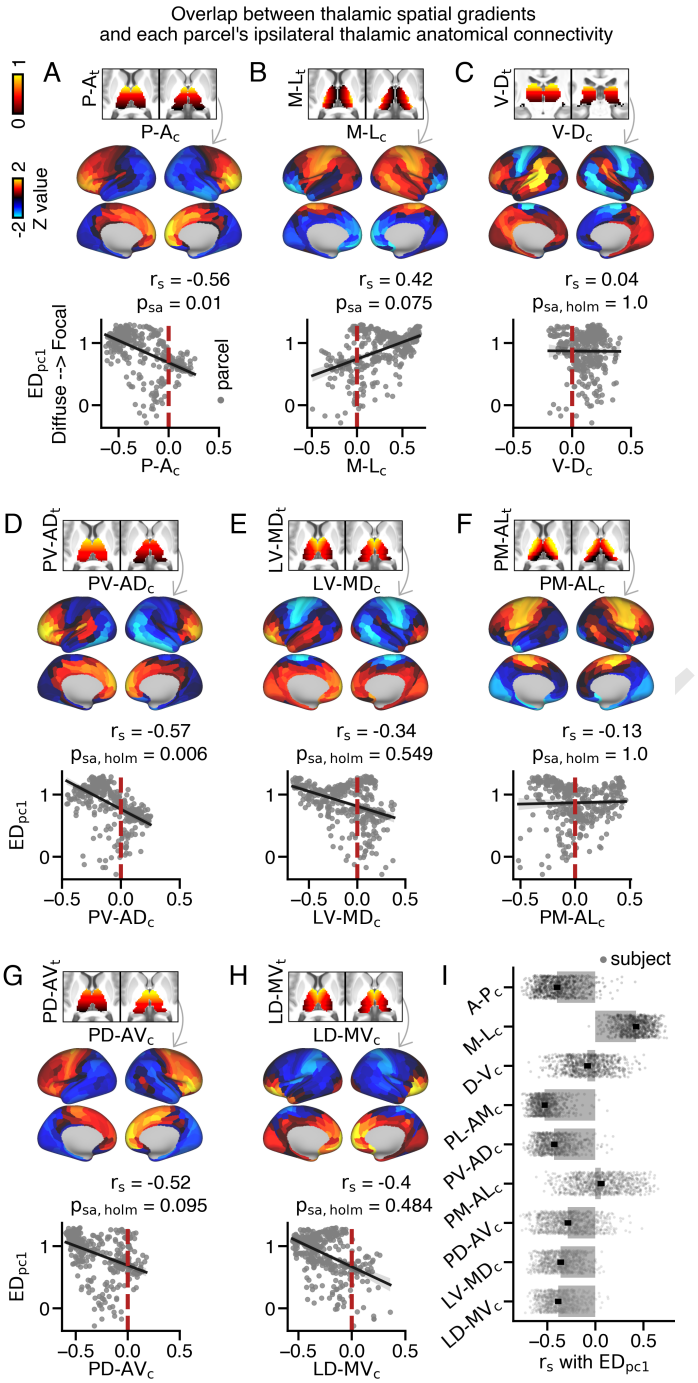

Fig. S28. Correspondence between ipsilateral ED_{pc1} loadings and thalamic spatial gradients. **(A-H)** Overlap between cortical parcel's thalamic anatomical connectivity and each thalamic spatial gradient: **(A)** Anteroposterior $(P\text{-}A)$, **(B)** Mediolateral $(M\text{-}L)$, **(C)** Dorsoventral $(D\text{-}V)$, **(D)** Posteroventral-Anterodorsal $(PV\text{-}AD)$, **(E)** Lateroventral-Mediodorsal $(LV\text{-}MD)$, **(F)** Posteromedial-Anterolateral $(PM\text{-}AL)$, **(G)** Posterodorsal-Anteroventral $(PD\text{-}AV)$, and **(H)** Laterodorsal-Medioventral $(LD\text{-}MV)$. **(I)** Consistent correspondence between ED_{pc1} loadings and thalamic spatial gradients across individual subjects: $A\text{-}P_c$ (median: -0.42), $M\text{-}L_c$ (median: 0.43), $D\text{-}V_c$ (median: -0.09), $PL\text{-}AM_c$ (median: -0.54), $PV\text{-}AD_c$ (median: -0.45), $PM\text{-}AL_c$ (median: 0.05), $PD\text{-}AV_c$ (median: -0.31), $LV\text{-}MD_c$ (median: -0.37), $LD\text{-}MV_c$ (median: -0.40).

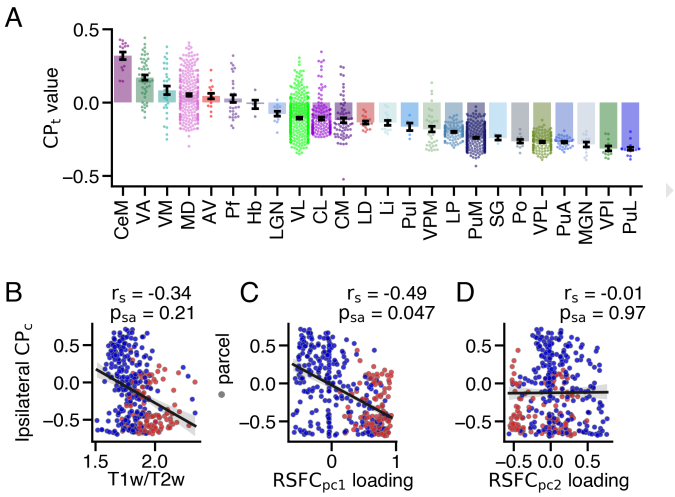

Fig. S29. Correspondence between cortical CP_c values and other measures. **(A)** Distribution of CP_t values for each thalamic nucleus. **(B)** CP_c values across cortex did not correspond with T1w/T2w values. **(C)** CP_c values across cortex showed a strong correlation with $RSFC_{pc1}$ loadings. **(D)** CP_c values across cortex did not correspond with $RSFC_{pc2}$ loadings.

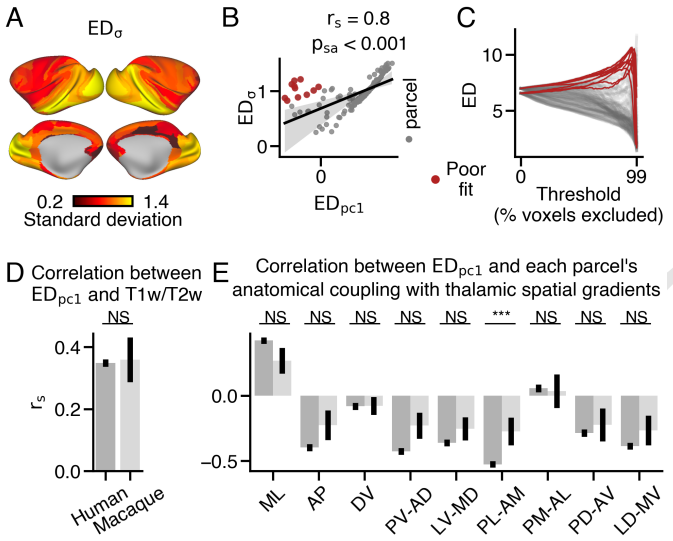

Fig. S30. Comparisons between human and macaque cortical connectivity patterns. **(A)** Macaque cortical map showing the standard deviation of ED (ED_σ) across thresholds for each cortical parcel. **(B)** Strong correlation between ED_{pc1} loadings and ED_σ values. Some cortical parcels (red dots) show a poor fit to the linear model. **(C)** ED matrix highlighting cortical parcels with poor correspondence between ED_{pc1} and ED_σ values. **(D)** Comparison of the correlation between ipsilateral ED_{pc1} loadings and T1w/T2w values between humans (median: 0.35) and macaques (median: 0.36), showing no significant difference between species. **(E)** Comparison of the correlation between ipsilateral ED_{pc1} loadings and each thalamic spatial gradient between humans and macaques. There was a significant effect of gradient and species, but no interaction. A trending difference was observed in the correlation with the PL-AM thalamic gradient between humans and macaques. No other significant differences were found between species.

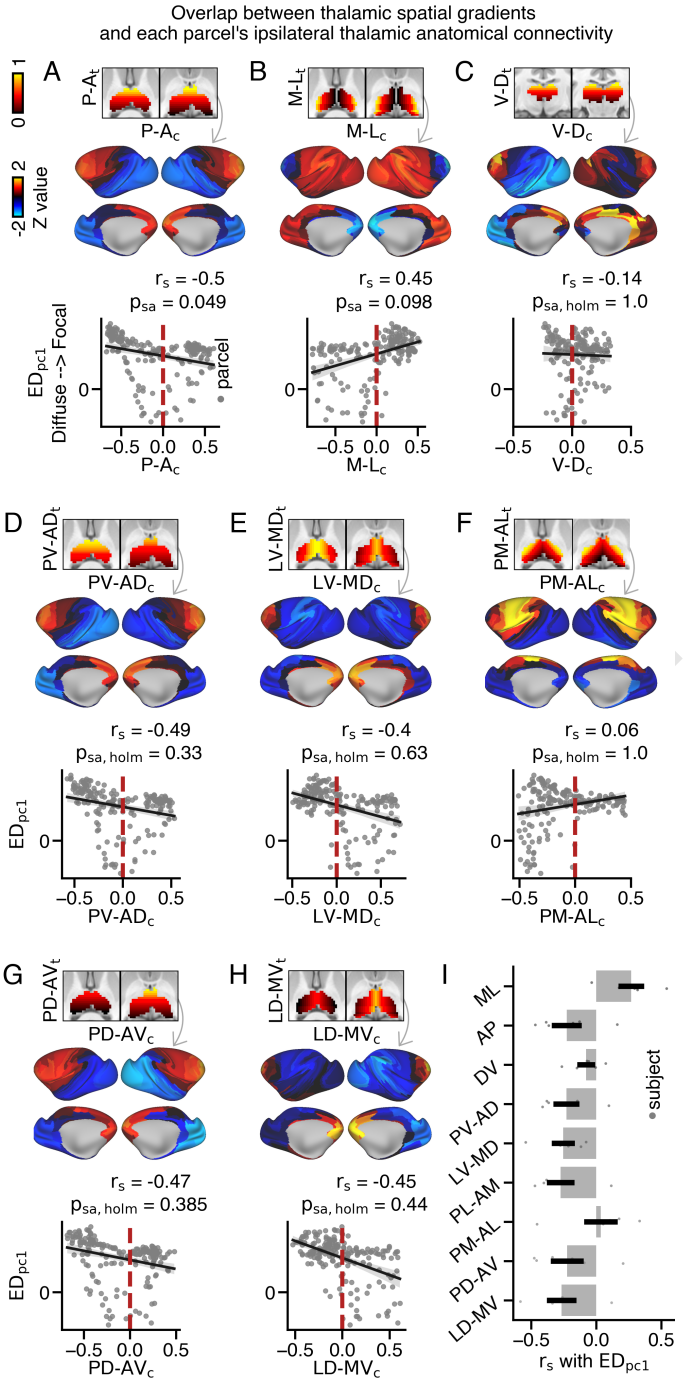

Fig. S31. Overlap between macaque thalamic spatial gradients and ipsilateral ED_{pc1} loadings. **(A)** Anteroposterior $(P\text{-}A)$ **(B)** Mediolateral $(M\text{-}L)$ **(C)** Dorsoventral $(D\text{-}V)$ **(D)** Posteroventral-Anterodorsal $(PV\text{-}AD)$ **(E)** Lateroventral-Mediodorsal $(LV\text{-}MD)$ **(F)** Posteromedial-Anterolateral $(PM\text{-}AL)$ **(G)** Posterodorsal-Anteroventral $(PD\text{-}AV)$ **(H)** Laterodorsal-Medioventral $(LD\text{-}MV)$ thalamic gradients. **(I)** Median correlation between ED_{pc1} and thalamic spatial gradients across individual macaque subjects: $P\text{-}A_c$ (median: -0.27), $M\text{-}L_c$ (median: 0.31), $D\text{-}V_c$ (median: -0.06), $PL\text{-}AM_c$ (median: -0.33), $PV\text{-}AD_c$ (median: -0.27), $PM\text{-}AL_c$ (median: 0.08), $PD\text{-}AV_c$ (median: -0.26), $LV\text{-}MD_c$ (median: -0.24), $LD\text{-}MV_c$ (median: -0.29).